membranes

MDPI

Article

Enhancing Oligopeptide-215 Skin Lipid Bilayer Diffusivity via Other Anti-Aging Peptides: A Molecular Dynamics Simulation Study

Choon-Peng Chng [1], Lu Zhang [2], Shikhar Gupta [2,*] and Changjin Huang [1,*]

[1] School of Mechanical and Aerospace Engineering, Nanyang Technological University, Singapore 639798, Singapore; choonpeng.chng@ntu.edu.sg
[2] P&G Singapore Innovation Center (SgIC), 70 Biopolis Street, Singapore 138547, Singapore
* Correspondence: gupta.s.50@pg.com (S.G.); cjhuang@ntu.edu.sg (C.H.)

Abstract

Efficient delivery of bioactive hydrophilic peptides across the stratum corneum (SC) is a major challenge due to the restricted permeation by the highly ordered lipid matrix, particularly for large or polar molecules. Oligopeptide-215 (OP215) is a biomimetic peptide with reported benefits in promoting cellular repair through enhanced proliferation, adhesion, and migration, but its size and polar/charged residues may limit transport through the SC. Here, we used atomistic molecular dynamics (MD) simulations to investigate whether caffeoyl hexapeptide-9 (CH-9), an anti-aging peptide-caffeic acid conjugate with enhanced skin permeation, can improve OP215 diffusivity across an SC lipid bilayer model. Both OP215 and CH-9 adsorbed onto the bilayer surface and partially inserted below the lipid headgroup region, with OP215 insertion mediated primarily by methionine sidechains and CH-9 insertion by the caffeoyl group. In the co-peptide system, CH-9 co-clustered with OP215 and modestly disrupted free fatty acid packing within the SC lipid bilayer. Position-dependent diffusivity calculations further showed that CH-9 increased the effective diffusivity of OP215 across the bilayer interior by approximately 13%, primarily by enhancing local diffusivity just below the bilayer surface. These results suggest that on top of being an effective anti-aging peptide, CH-9 may act as a permeation-enhancing co-peptide by inducing lipid packing disorder, thereby facilitating OP215 diffusion through the SC lipid matrix. This research provides molecular-level insight into the design of multi-peptide systems for improved topical delivery of functional skincare peptides.

Keywords: skin permeation; stratum corneum; biomimetic peptides; anti-aging; molecular diffusivity

Check for updates

Academic Editors: Yukihiro Okamoto, Haoyuan Jing and Yanbin Wang

Received: 16 September 2026
Revised: 19 October 2026
Accepted: 21 October 2026
Published: 23 October 2026

Copyright: © 2026 by the authors. Licensee MDPI, Basel, Switzerland. This article is an open access article distributed under the terms and conditions of the Creative Commons Attribution (CC BY) license.

1. Introduction

Peptides are essentially short sequences of amino acids that carry out various biological functions. Use of peptides as therapeutics have various advantages such as biocompatibility, high selectivity, low toxicity, high mechanical stability, and ease of synthesis, to name a few [1–3]. Peptides have been adopted as skin-targeting molecules for various purposes, including anti-aging, wound healing, and the treatment of skin disorders [4–9]. However, natural peptides face several limitations as therapeutic agents: they are susceptible to proteolytic degradation and oxidative instability, and they typically exhibit poor membrane permeability due to the abundance of charged and polar amino acid residues and their relatively large size [2]. Hence, modifications of peptide backbone or amino acids,

and conjugation of moieties, have been undertaken to improve stability and membrane permeability [3].

To deliver a therapeutic peptide or any small-molecule drug into the skin, the peptide or molecule would have to transverse across the outermost layer of the skin epidermis known as the stratum corneum (SC). The SC protects the skin against water loss, injury and exogeneous substances that may be harmful, and thus serves as the main barrier to the transdermal delivery of therapeutic molecules for skincare [10,11]. The SC consists of multiple layers of dead corneocytes surrounded by lipid-enriched intercellular domains [12]. The intercellular domains are considered to be the primary permeation passage for any molecules, as the domains are continuous throughout the SC [12,13]. The lipid-enriched domains are composed of highly saturated long-chain ceramides (hydrocarbon chains ranging from 16 to 32 carbon atoms) and free fatty acids (FFAs; hydrocarbon chains ranging from 16 to 34 carbon atoms) [10,14,15]. Together with cholesterol, the intercellular domains are highly ordered, gel-phase membranes [11,16,17]. Such an organization of lipid species confers the barrier property of the SC but also makes it challenging for compound delivery into the SC, especially for hydrophilic compounds.

Oligopeptide-215 (OP215), a biomimetic peptide derived from frog skin secretions, was believed to promote wound healing and cellular repair via enhanced cell proliferation and was found to restore skin barrier homeostasis through the concurrent modulation of JAK-STAT and NF-κB signaling pathways [9]. By replacing the oxidation-susceptible cysteine residue in the parent peptide CW49 with methionine, the thermodynamic stability was much improved without affecting the biological function. However, as OP215 contains 11 amino acid residues and has a molecular weight of 1254 Da, it is a rather large molecule for skin permeation. Compounds heavier than 500 Da (>about 6 amino acids) are known to have very low diffusivities across the skin [18]. Furthermore, OP215 contains a large and positively charged Arginine residue as well as polar residues Threonine and Glutamine, also making the peptide unfavorable for the apolar interior of the SC lipid matrix. Hence, OP215 may have limited skin permeability.

We have previously presented the design, synthesis and anti-photoaging properties of a cosmetic peptide-caffeic acid conjugate, caffeoyl hexapeptide-9 (CH-9) [8]. Hexapeptide-9 (H-9) is a well characterized synthetic collagen-mimetic peptide with anti-aging properties with the sequence Gly-Pro-Gln-Gly-Pro-Gln, which mimics specific fragments of human collagen. Caffeic acid is a phenolic compound widely used in cosmetics for its antioxidant, anti-inflammatory and photoprotective properties [19]. As H-9 peptide is highly susceptible to enzymatic degradation [6], and caffeic acid has poor water solubility and dermal absorption [20], we have shown that CH-9 effectively overcame these limitations and exhibited superior anti-photoaging and transdermal efficiency compared to H-9 [8]. Given the success of CH-9, we would like to investigate whether a co-peptide system of CH-9 and OP215 could enhance the molecular diffusivity of OP215 compared to OP215 alone across the SC lipid bilayer.

Molecular dynamics (MD) simulations, whereby detailed interactions between molecules are calculated by solving Newton's equation of motion, have offered important physical insights into the interaction of various peptides with phospholipid bilayers [21–23], the atomistic structure of SC lipid bilayers [24,25], and also the permeation of small molecules through the SC lipid bilayers [26–28]. In this study, we employed MD simulations to model the detailed interaction between OP215 peptides with an SC lipid bilayer model, in the absence or presence of CH-9 peptides. We found that both OP215 and CH-9 can partially insert under the bilayer surface via methionine sidechains for OP215 and via the caffeoyl group for CH-9. The OP215/CH-9 co-peptide system was found to slightly reduce the lipid packing of FFAs in the SC lipid bilayer compared to the OP215-only system.

We have also calculated the diffusivity of OP215 across the SC lipid bilayer for both systems and found a significant increase of about 13% in the effective diffusivity in the co-peptide system, whereby the local diffusivity just below the bilayer surface is enhanced. Hence, the presence of CH-9 may induce lipid packing disorder, which enhanced the diffusion of OP215 across the SC lipid bilayer.

2. Materials and Methods

2.1. Generation and Equilibration of SC Lipid Bilayer Model

The SC lipid bilayer model is the same as we have previously constructed and equilibrated [29]. Briefly, the lipid bilayer consists of 100 molecules of ceramide Cer24 NS (C24:0 fatty acid tail and C18:1 sphingosine tail), 100 molecules of cholesterol and 100 molecules of protonated FFA (with equal numbers of C16:0/palmitic acid, C18:0/stearic acid and C20:0/arachidic acid) generated with PackMol version 20.15.3 software [30]. The CHARMM-GUI webserver was used to obtain CHARMM36 force-field parameters for the lipids [31,32]. GROMACS MD simulation package version 2023 was used for energy minimization and MD simulations [33–35].

2.2. Generation of Peptide Models and Simulation of Peptide–SC Lipid Bilayer Interactions

The three-dimensional coordinates of each peptide was generated using Accelrys Discovery Studio version 4.5 (for CH-9) or using Avogadro software version 1.2.0 (for OP215) and input into the CHARMM-GUI webserver, which generated the all-atom CHARMM36 force-field (FF) parameters for the CH-9 and OP215 peptides [31,32]. CH-9 combined parameters based on CHARMM Generalized FF (CGenFF) for the caffeoyl group using CHARMM-GUI Ligand Reader & Modeler with H-9 peptide parameters based on standard CHARMM FF and was studied previously [8]. The OP215 peptide was simulated using GROMACS in a periodic simulation box filled with TIP3 water models, and the system was electrically neutralized with potassium and chloride ions at 0.15 M concentration. After energy minimization to relax any possible steric clashes and 125 ps of simulation with peptide-heavy atoms restrained, unrestrained simulation was then carried out with a 2 fs simulation time-step for 100 ns under a temperature of 303 K and pressure of 1 bar. Electrostatic interactions were computed using the Particle Mesh Ewald method with a cut-off distance of 1.2 nm. Van der Waals (vdW) interactions were computed using a cut-off method with forces smoothly switched to zero between 1.0 and 1.2 nm. For post-processing, Visual Molecular Dynamics (VMD) software v1.9.4 was used for visualization of the simulation trajectories, and the GROMACS tool was used to calculate the temporal evolution of the radius of gyration of OP215.

For simulation of peptide interactions with other peptides and with SC lipid bilayer, two copies of OP215 peptides (taken from 50 ns simulation snapshot in water showing compact configuration) were randomly placed in the aqueous phase above the bilayer for the "OP215 only" system. For the "OP215 with CH-9" system, 10 copies of previously simulated CH-9 peptides followed by two copies of OP215 peptides were randomly placed above the bilayer. Because OP215 peptides were placed after CH-9, the initial positions of OP215 in the latter system were not the same as that in the former system. Energy minimization and positional restrained simulation with decreasing restraints on the lipid head-groups was performed. Production simulation was then performed at 310 K and 1 bar for 300 ns, with a Nose–Hoover thermostat with time constant of 1 ps and semi-isotropic pressure coupling with the Parrinello–Rahman barostat with a time constant of 5 ps and compressibility of 4.5×10^{-5} bar^{-1}. Electrostatic and vdW interactions were calculated as above.

To monitor the adsorption of peptides onto the SC lipid bilayer surface, the shortest distance along the Z-axis (bilayer normal) of each peptide atoms and bilayer midplane (defined using the average position of the last carbon atom along arachidic acid chains) was calculated using an in-house VMD script. For peptides that bind to the bottom leaflet of the bilayer, the distance turned out to be negative and was converted to a positive value. The final shortest distances from the bilayer midplane for each peptide were averaged. The GROMACS "gmx order" command was used to calculate the order parameter S_{cd}. For the CH-9-only system, simulation data (0–100 ns) was taken from [8].

The area per lipid of the SC lipid bilayer was calculated from the time-averaged (200–300 ns) bilayer X-Y projected area divided by half the number of lipids (cholesterol excluded). The bilayer thickness was calculated by taking the difference between the average Z-coordinates of Cer24 NS head-group N atoms in the top and bottom monolayers and then averaging this difference over time as in a previous study [36]. The area compressibility modulus measuring the resistance of the bilayer to in-plane stretch was computed based on the fluctuation of the bilayer X-Y projected area as $K_A = k_B T\langle A\rangle / \langle \delta A^2 \rangle$, where $\langle A\rangle$ is the average projected area, $\langle \delta A^2 \rangle$ is the mean square fluctuation, k_B is the Boltzmann constant and T is the temperature in Kelvin [37,38]. The Spatial (2D) lipid order parameter was calculated using MOSAICS v1.1 software with the "p2_mpi" command for the rank 2 order parameter using 200–300 ns simulation data and for the top and bottom leaflets separately [39]. Mass density profiles of water, palmitic acid, stearic acid, arachidic acid and peptides were calculated using the GROMACS "gmx density" command.

2.3. Calculation of Position-Dependent Diffusivity of Peptides Across the SC Lipid Bilayer

For the calculation of position-dependent diffusivity, we utilized a similar approach to generate configurations for position-dependent diffusivity calculations from our previous studies [29,40]. One of the peptides bound on the bilayer surface was selected from the final simulation configuration and pulled into the bilayer center (as well as away from the surface) to generate configurations at various depths (along Z) relative to the bilayer center. To do this, the GROMACS pull code was used where a virtual spring with a spring constant of 1000 kJ/mol/nm^2 was moved at a rate of 0.005 nm/ps. Next, umbrella sampling was performed at each of these Z-positions for 40 ns with a force constant of 2000 or 3000 kJ/mol/nm^2 to maintain the peptide Z-positions. To avoid any lipids being pulled into the bilayer interior and changing the polarity of the bilayer interior during pulling and umbrella sampling simulations, the headgroup atom of each lipid was restrained in the Z-location with a spring constant of 200 kJ/mol/nm^2. Constrain forces were stored at every 0.1 ps during the last 10 ns of each sampling simulation and then used to calculate the following position-dependent diffusivity in terms of a time correlation function involving constrain forces [26]:

$$\mathrm{D(z)} = \frac{(\mathrm{RT})^2}{\int_0^\infty \langle \Delta \mathrm{F(z,t)} \Delta \mathrm{F(z,0)} \rangle \mathrm{dt}} \tag{1}$$

where R is the gas constant, T is temperature in Kelvin, and $\Delta F(z,t) = F(z,t) - \langle F(z,t)\rangle$ is the instantaneous deviation of the constrain force from the average value over time $\langle F(z,t)\rangle$. The time correlation function in the denominator of D(z) was written as a time integral over different starting times t′,

$$\langle \Delta \mathrm{F(z,t)} \Delta \mathrm{F(z,0)} \rangle = \lim_{\mathrm{T}\to\infty} \frac{1}{\mathrm{T}} \int_0^{\mathrm{T}} \Delta \mathrm{F}\left(\mathrm{z,t'}\right) \Delta \mathrm{F}\left(\mathrm{z,t'+t}\right) \mathrm{dt'} \tag{2}$$

The algorithm to compute D(z) was implemented in Python3 using the NumPy library.

For improved sampling, we repeated the procedure using simulation snapshots at 200 ns and 300 ns using each of the two OP215 peptides. Each peptide was pulled from the

surface into the bilayer center as well as away from the surface and across to the opposite surface. D(z) values calculated at similar z-positions on either side of the bilayer midplane were then averaged for the 300 ns profile. Furthermore, for z = 0 nm and 0.1 nm, the umbrella sampling simulations were extended to 50 ns and again the last 10 ns was used. To characterize the difference in overall diffusivity in the bilayer interior and avoiding any bias due to unequal spacing of data along z, we calculated the effective diffusivity (D_{eff}) by matching the area under each profile from 0 to 2.5 nm (or −2.5 nm to 0 nm) to a rectangular area of side D_{eff} and 2.5 nm. The area under each profile was calculated as the sum of trapezoidal areas. D_{eff} values estimated from each (half) profile for each system (OP215 only or OP215 with CH-9, 200 ns and 300 ns configurations) were then averaged.

3. Results

3.1. Peptide Adsorption onto SC Lipid Bilayer and Penetration Below Lipid Headgroups

We performed MD simulations to understand how OP215 peptides interact and bind onto a model SC lipid bilayer in the absence and presence of CH-9 (Figure 1). The same SC lipid bilayer model was used as we have previously [29], which has Ceramide24 NS, FFAs and cholesterol in equimolar ratios. OP215 is an amphiphilic 11-amino acid peptide, whereas CH-9 is a polar hexapeptide with a caffeoyl group attached and exhibits both enhanced skin permeation in vivo and improved insertion into an SC lipid bilayer in silico compared to H-9 [8].

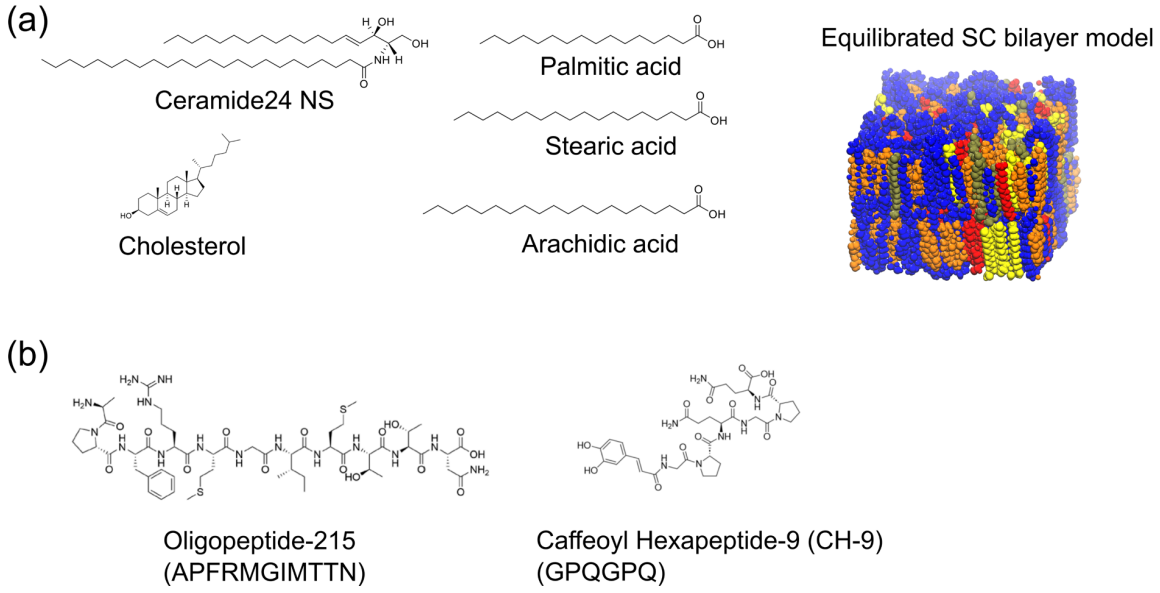


Figure 1. All-atom model of stratum corneum (SC) lipid bilayer interacting with skin-targeting peptides. (**a**) Chemical structures of the lipids present in our SC lipid bilayer model. The numbers of ceramide24 NS, cholesterol and protonated FFA molecules are at 1:1:1 ratio. The three FFAs are also present in equimolar ratio. Ceramides and cholesterol are colored blue and orange, respectively, while FFAs are colored as follows: palmitic acid in yellow, stearic acid in red and arachidic acid in olive. Water layers above and below the bilayer are omitted for clarity. (**b**) Chemical structures of the two short peptides considered in this study.

First, an OP215 peptide was simulated in water for 100 ns and the configuration at 50 ns was extracted and used for simulation with the SC lipid bilayer, as the configuration is more compact with a small radius of gyration (R_g) (Figure 2a). Next, two OP215 peptides were placed slightly above the SC bilayer surface in the OP215-only system, and the peptide–SC lipid interaction was simulated for 300 ns (Figure 2b). OP215 peptides were observed to adsorb onto the bilayer surface, and peptide atoms inserted slightly below the

SC lipid headgroup region (see inset in Figure 2b). One OP215 peptide bound quickly to the top surface whereas the other OP215 peptide crossed the top periodic boundary and adsorbed onto the bottom surface. Thereafter, both peptides remained stably bound to the bilayer (Figure 2c). Peptide atoms were able to reach below the SC lipid headgroup region (denoted by ceramide NF atoms) and reach close to ceramide C9F atoms (8th carbon along the fatty acid chain counting from the carbonyl carbon) located 1.5 nm from the bilayer midplane or 0.8 nm below the bilayer surface (Figure 2c). We found that methionine (a hydrophobic residue) at position 5 or 8 is the part of the peptide that inserts the deepest below the lipid headgroup atoms.

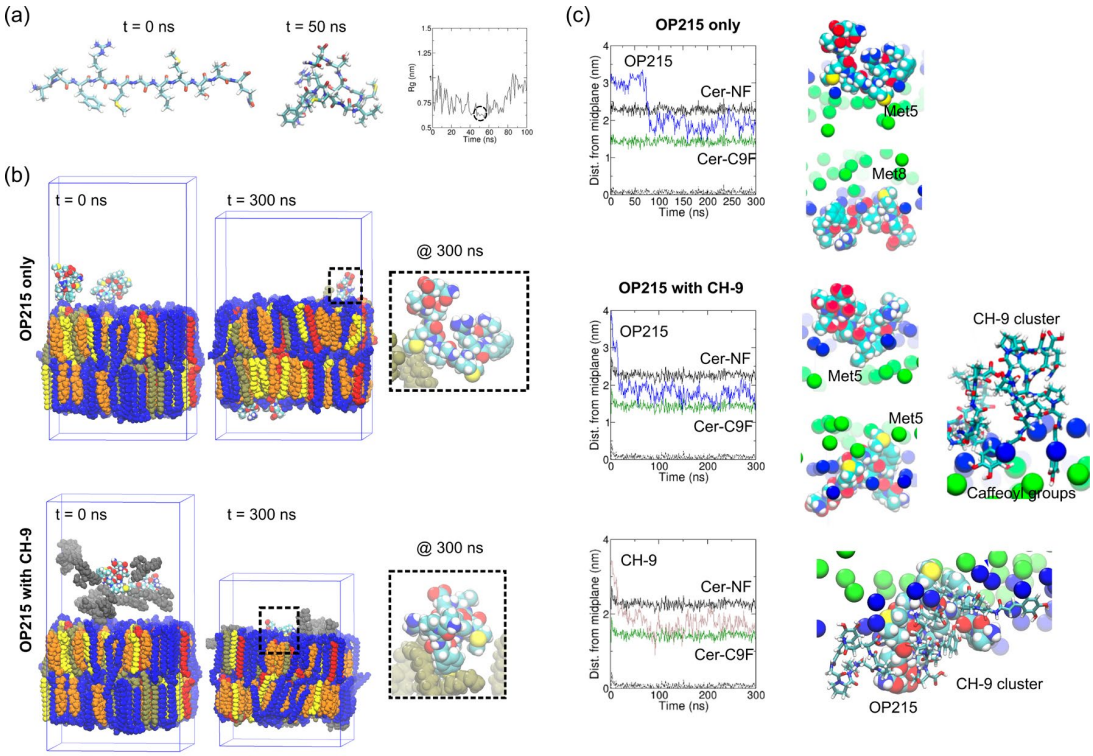


Figure 2. MD simulations of the interaction between OP215 peptides and the equilibrated SC lipid bilayer. (**a**) Left Model of OP215 peptide before MD simulation (t = 0 ns). Peptide is shown in stick representation with atoms colored as follows: carbon in cyan, oxygen in red, nitrogen in blue, sulphur in yellow and hydrogen in white. Middle Selected model of OP215 (at t = 50 ns) for simulation with SC lipid bilayer on the basis of compactness, i.e., low values for radius of gyration (R_g) shown on Right with circle at t = 50 ns, in order to pack more peptides on the SC bilayer surface. (**b**) Simulation snapshots showing the initial and final configurations of the peptides relative to the SC bilayer surface for model with only OP215 or with OP215 and CH-9. Water molecules on either side of the bilayer are omitted for clarity. In the system with CH-9, the 10 copies of CH-9 included are shown in gray. Periodic simulation box shows changes in dimensions during simulation as the molecules rearrange. Zoomed-in views show snapshots of OP215 peptide on the bilayer surfaces (only arachidic acid molecules are shown for clarity and in olive as in Figure 1). (**c**) The temporal evolution of the minimum distance along bilayer normal (z-axis) between peptide atoms and the middle of SC lipid bilayer (based on terminal carbons of arachidic acids, black dashed line) showing depth of penetration of the peptides, averaged over all peptides of the same type (OP215 or CH-9). The z-position of ceramide head-group nitrogen atom (Cer-NF, black line) demarcates the bilayer surface whereas the z-position of ceramide carbon atom (Cer-C9F, green line) provides a guide to the degree of bilayer penetration of the peptides. Final simulation snapshots of individual OP215 peptides and CH-9 cluster of three peptides are also shown with Cer-NF and Cer-C9F atoms in blue and green, respectively.

For the system with CH-9 peptides, 10 CH-9 and two OP215 peptides were placed randomly above the SC lipid bilayer. The CH-9 peptide configuration was taken from our previous study [8]. Here, both OP215 and CH-9 peptides adsorb onto the bilayer surface. The degree of bilayer penetration for OP215 is slightly higher for this system (Figure 2c). Similarly, methionine at position 5 was observed to be the part of the OP215 peptide that is deepest into the bilayer. CH-9 peptides form clusters, and caffeoyl groups were observed to insert below the bilayer headgroups. The caffeoyl groups of CH-9 inserted deepest into the bilayer, showing up as dips in the minimum distance between CH-9 and the bilayer midplane (Figure 2c). Caffeoyl groups were also found to orient towards the SC bilayer surface, and CH-9 showed stronger interaction energy with SC lipids than H-9 in our previous study [8]. CH-9 also showed enhanced skin permeation in vivo compared to H-9 [8], with the enhancement being attributed to the caffeoyl group conjugation.

To understand the interaction among the molecular species, we also calculated the interaction energies between OP215 peptides and SC lipids, between CH-9 peptides and SC lipids, and between OP215 and CH-9 peptides (Figure S1a). Although the average total interaction energy (coulombic + dispersive) between an OP215 peptide and SC lipids is lower in the system with CH-9 compared to the system with OP215 only, this is because the OP215 peptides also interact with CH-9. This resulted in co-clustering of OP215 with CH-9. CH-9 peptides also interact with SC lipids to a larger degree than CH-9 interaction with OP215. In terms of the total interaction energies between all peptides (OP215 or CH-9) and SC lipids (Figure S1b,c), CH-9 interaction with SC lipids is quite strong and stable. We also computed the interaction energies between each OP215 peptide and each CH-9 peptide. The energies of interacting OP215–CH-9 pairs are shown in Figures S2 and S3 for each of the two OP215 peptides, which show contributions of both coulombic interaction and vdW (LJ) interactions. Simulation snapshots taken during the interaction windows are also shown, which suggest that the OP215–CH-9 interactions are mostly hydrogen bonds, which have both coulombic and vdW components involving hydrophilic sidechains and backbone atoms (Figures S2 and S3). Cation-Pi interaction between Arg sidechain of OP215 and the caffeoyl group of CH-9 was also observed (Figure S2, 100 ns and 125 ns snapshots). Hence, OP215 interactions with CH-9 are hydrophilic in nature.

3.2. CH-9 Adsorption onto SC Lipid Bilayer Perturbs the Bilayer and Enhances Diffusivity of OP215 Across the Bilayer

How does the presence of CH-9 on the SC lipid bilayer modulate the bilayer and the absorption/insertion of another peptide such as OP215? The FFA lipid order parameter that reflects the packing of lipids in the bilayer showed some differences between the systems with OP215 only, OP215 with CH-9 and CH-9 only (Figure 3). Order parameters (S_{cd}) for palmitic acid (C16:0) and stearic acid (C18:0) are lower in the presence of CH-9, whereas the order parameter for arachidic acid (C20:0) is the same in the presence of CH-9. The lowering of S_{cd} is especially pronounced in the palmitic and stearic acid head-group regions (low atom numbers) in the presence of CH-9 (both "OP215 with CH-9" and "CH-9 only") due to insertion of the caffeoyl group. This suggests that the lipids in the SC bilayer containing CH-9 might be slightly more disordered and more loosely packed, and the disruption level is highly dependent on the FFA chain length with the most severe disruption to the shortest FFA. We also calculated 2D maps of the lipid order parameter using all three FFAs and ceramides for the OP215-only and OP215 with CH-9 systems (Figure S4), which show a lower order parameter in the latter system. The reduction in lipid order is over a wide region but not completely over the entire bilayer, as revealed by regions of higher order parameters.

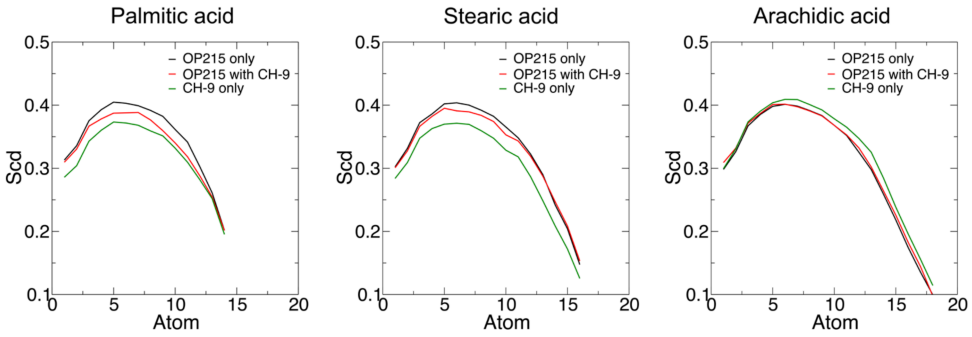


Figure 3. Free fatty acid carbon chain order parameters (averaged over lipids and 200–300 ns simulation time) for the systems OP215 only, OP215 with CH-9, and CH-9 only.

Mass density profiles indicate no water penetration during the 200–300 ns simulation of OP215 with CH-9 (or OP215 only) (Figure S5a,b). Furthermore, the density of the peptides indicates that OP215 peptides are bound slightly deeper on the bilayer surface in the system with CH-9 (Figure S5c vs. S5d). The density profiles for the FFAs are very similar with or without CH-9 though slightly lower, just below the head-group regions for palmitic and stearic acid densities (around 2 nm from bilayer center) (Figure S5e), in agreement with lipid order parameter plots in Figure 3.

Characterization of the physical properties of the SC bilayers in each system further revealed that, although both bilayers have very similar areas per lipid and similar average thicknesses, the area compressibility modulus is relatively smaller for the bilayers with CH-9 (Table 1). This is consistent with the lipid order parameter results presented above, indicating that CH-9 perturbs the bilayer and reduces its compactness and stiffness.

Table 1. Physical properties of the SC lipid bilayers with OP215 and/or CH-9.

System	Area/Lipid (nm^2)	Bilayer Thickness (nm)	Area Compressibility Modulus (mN/m)
OP215 only	0.49	4.53 ± 0.03	2765
OP215 with CH-9	0.49	4.55 ± 0.03	2349
CH-9 only	0.49	4.57 ± 0.03	2353

To reveal how binding of CH-9 to the SC lipid bilayer might modulate the trans-bilayer diffusion of OP215, we computed the positional diffusivity of OP215 peptide along the bilayer normal from outside ($|z| \geq 4$ nm) to the center of the bilayer (z = 0 nm). Positional diffusivities averaged over both sides of the bilayer and then reflected about z = 0 nm based on 300 ns configurations are shown in Figure 4, whereas the original profiles across the bilayer are shown in Figure S6. As expected, the averaged diffusivity profiles show similar diffusivity values for OP215 outside the bilayer in bulk water ($|z| \geq 4$ nm) as CH-9 are all bound to the bilayer. As the OP215 peptides approach the bilayer surface, the diffusivity value decreases as observed from diffusivity profiles calculated for many small polar/apolar molecules [26]. Near the bilayer surface at between 2.5 to 3 nm, interaction with polar lipid headgroups and CH-9 peptides reduces D(z). Below 2.5 nm, the peptide enters the bilayer interior with higher density (due to the lipid packing) than in water. For the OP215 peptide in the OP215-only system, D(z) further reduces slightly but starts to increase near the bilayer center. This may be due to more free volume or less density at the middle of the bilayer, as shown for a similar SC lipid bilayer [26]. In contrast, for the OP215 peptide in the OP215 + CH-9 system, D(z) increases just below the bilayer surface (1.5 nm < $|z|$ < 2.5 nm) before decreasing to a similar value as in the OP215-only system.

Again, D(z) shows a peak in the center as in the OP215-only system. The effective diffusivity (D_{eff}) was then obtained by matching the area under each profile (z = −2.5 nm to 0 nm or from 0 to 2.5 nm) to a rectangular area of side D_{eff} and 2.5 nm (Figure S6). The averaged D_{eff} from four areas (two each from the 200 ns and 300 ns profiles) is $1.09 \times 10^{-7} \pm 3.55 \times 10^{-8}$ cm^2/s and $1.23 \times 10^{-7} \pm 4.10 \times 10^{-8}$ cm^2/s for the OP215-only and OP215 + CH-9 systems, respectively, representing a 13% relative increase for the system with CH-9 over the OP215-only system.

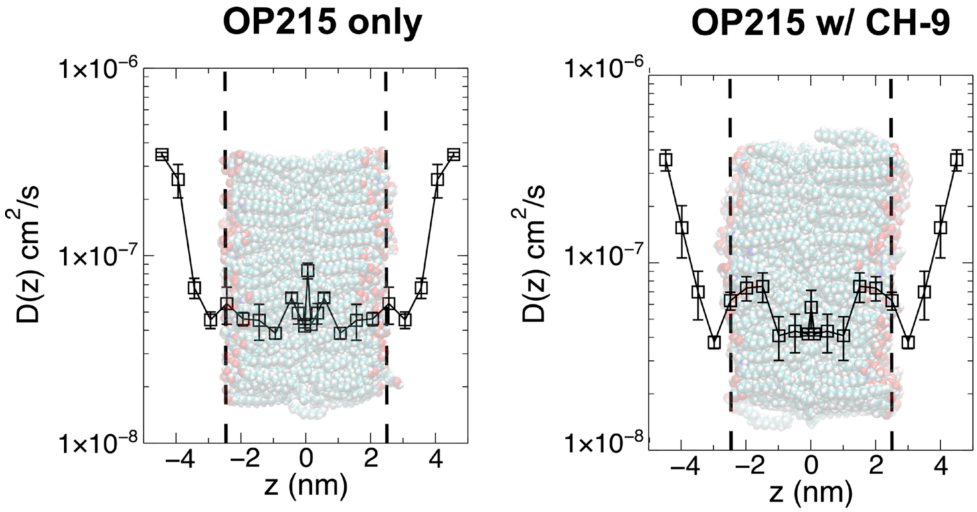


Figure 4. Comparison of the diffusivity profiles across the SC lipid bilayer for OP215 peptides in the absence (**Left**) and presence of CH-9 peptides (**Right**), calculated using configurations at 300 ns from each system. The distance to the peptide center-of-mass from the center of the lipid bilayer is denoted by z. Dashed vertical lines mark the locations of the bilayer surface determined based on the bilayer thickness and bilayer center, with an image of the respective bilayer configuration superimposed. Each data point is an average over two umbrella sampling simulations performed at ±z value (i.e., on either side of the bilayer midplane). The profile for $z \geq 0$ nm is then reflected about z = 0 nm, assuming the bilayer is symmetric in lipid composition.

4. Discussion

Despite the many strengths of peptides as skin-targeting actives, they suffer from the challenges of skin permeation due to incompatibility between the polar amino acids in the peptides and the apolar environment of the lipid-enriched intercellular domains in the SC. Various strategies such as cyclization and conjugation to hydrophobic moieties (e.g., fatty acid chains and caffeic acid) have been proposed to improve the skin permeability of therapeutic peptides [3,7,41]. Other techniques to enhance skin permeability of peptides include the use of chemical enhancers, physical enhancers (e.g., microneedles, iontophoresis), encapsulation in liposomes or liquid crystal nanoparticles, etc. [41,42]. Here, we proposed an alternative strategy that involves a co-peptide system whereby a caffeic acid-conjugated peptide (CH-9), previously found to show improved SC bilayer insertion over H-9 [8], may act as a chemical enhancer to increase the diffusivity across the SC bilayer of an unmodified peptide (OP215), which is hydrophilic with a large positively charged amino acid. This draws inspiration from our previous simulation work whereby amphiphilic skin brightening agents that are also known skin penetration enhancers improved the diffusivity of niacinamide (a polar, skin brightening agent) [40].

Using MD simulations, we investigated the adsorption of OP215 alone or OP215 together with CH-9 onto an SC lipid bilayer model. OP215 could partially insert under the polar lipid headgroups via its apolar methionine amino acid residues in both systems, and CH-9 inserts its caffeoyl group under the lipid headgroups. Although the degree

of insertion of OP215 in conjunction with CH-9 is at best marginally better than OP215 alone, quantification of the FFA chain lipid order parameter, which reflects the degree of lipid packing in the SC bilayer, reveals a small decrease in the lipid packing order in the presence of CH-9. Consistent with our observations, Villanueva et al. also reported peptide- and small-molecule-induced membrane perturbation using in vitro techniques, including Langmuir isotherms and differential scanning calorimetry [43]. Calculation of OP215 diffusivity across the SC bilayer for each system using umbrella sampling further suggests a different diffusivity profile whereby the diffusivity just under the lipid headgroups is higher in the presence of CH-9, which might be attributed to perturbation by CH-9. The effective diffusivity of OP215 also increases in the co-peptide system. Hence, CH-9 might indeed function as a skin permeation-enhancing co-peptide to facilitate OP215 diffusion through the SC lipids. Our research raises the possibility of designing multi-peptide systems that enhance topical delivery of skincare peptides that are either too large or too polar, resulting in low SC permeability, with one or more peptides acting as skin permeation enhancers.

This research adds specific value to the cosmetic and anti-aging field by providing a mechanistic basis for improving the topical delivery of functional skincare peptides, which often show promising biological activity but limited skin penetration due to their size and polarity. By demonstrating that CH-9 can act as a permeation-enhancing co-peptide for OP215 through localized perturbation of SC lipid packing and increased peptide diffusivity, this study supports a formulation strategy in which anti-aging peptides can enhance the delivery of another peptide without chemically modifying the active target. This is particularly relevant for next-generation cosmetic products aiming to improve skin barrier function, reduce visible signs of aging, and increase the bioavailability of peptide-based actives in the skin. However, our study has some limitations, including the use of a simplified SC lipid bilayer model with only one representative ceramide and three FFAs in order to reduce computational demands and model complexity, and the effects of CH-9 on lipid packing may depend strongly on lipid composition and bilayer organization. Hence, our model can only inform about the molecular diffusivity of the OP215 peptide across a single SC lipid bilayer, and the skin permeability enhancement of OP215 due to CH-9 would need to be demonstrated in future in vitro experiments such as measurements of OP215 skin permeability in Franz cell experiments [44]. Further, Langmuir films consisting of ceramide, cholesterol and FFA may be probed via various monolayer techniques to characterize the effect of OP215 alone and in conjunction with CH-9 in terms of changes in molecular area (surface pressure–molecular area isotherms) and surface compressibility modulus, which measures film stiffness/elasticity [45].

Nevertheless, the approach highlights MD simulations as a potentially useful tool for screening synergistic peptide combinations, guiding cosmetic formulation design, and accelerating the development of peptide-based anti-aging technologies with stronger scientific substantiation.

5. Conclusions

In this study, atomistic MD simulations were used to investigate whether CH-9 can enhance the permeation of OP215 across a model SC lipid bilayer. Our simulations revealed that the presence of CH-9 modestly perturbed the packing of FFAs in the SC lipid bilayer with a slight increase in lipid disorder. This structural perturbation was accompanied by an increase in the position-dependent diffusivity of OP215 just below the bilayer surface. Overall, the effective diffusivity of OP215 across the bilayer interior was enhanced by approximately 13% in the OP215 + CH-9 system. These findings suggest that CH-9 can function as a permeation-enhancing co-peptide by locally disrupting SC lipid packing and

facilitating OP215 diffusion through the lipid matrix. More broadly, the results support the potential of rationally designed multi-peptide systems to improve the topical delivery of functional skincare peptides that would otherwise exhibit limited permeability due to their size and polarity. Future experimental validation will be valuable to confirm the predicted enhancement in skin permeation and to guide further optimization of peptide combinations for topical applications. In vitro experiments, such as using Franz diffusion cells with artificial skin or skin explants that measure permeability of OP215 in the presence of CH-9, would be useful to validate our simulation findings [44]. Further study of CH-9 to identify any potential adverse effects on the skin may be carried out, such as increased trans-epidermal water loss (TEWL) due to lipid packing disruption or skin irritation.

Supplementary Materials: The following supporting information can be downloaded at: https://www.mdpi.com/article/10.3390/membranes16110355/s1, Figure S1: Interaction energies between peptides and SC lipids from each system; Figure S2: OP215 and CH-9 interaction energies and co-cluster snapshots for the first copy of OP215. Figure S3: OP215 and CH-9 interaction energies and co-cluster snapshots for the second copy of OP215; Figure S4: Spatial (2D) lipid order parameter maps using 200-300 ns of simulation data for (a) OP215-only and (b) OP215 with CH-9 systems using MOSAICS software; Figure S5: Mass density profiles; Figure S6: Comparison of the diffusivity profiles across the SC lipid bilayer for OP215 peptides in the absence (Left) and presence of CH-9 peptides (Right) using the 300 ns and 200 ns configurations from the respective simulations.

Author Contributions: Conceptualization, C.H., L.Z. and S.G.; methodology, C.-P.C.; software, C.-P.C.; validation, C.-P.C. and C.H.; formal analysis, C.-P.C.; investigation, C.-P.C.; resources, C.H.; data curation, C.-P.C.; writing—original draft preparation, C.-P.C.; writing—review and editing, C.H., S.G. and L.Z.; visualization, C.-P.C.; supervision, C.H.; project administration, C.H.; funding acquisition, C.H. and S.G. All authors have read and agreed to the published version of the manuscript.

Funding: This research is supported by A*STAR under its Industry Collaboration Projects (IAF-ICP)-Research and Innovation Partnership with P&G-Joint Fund (I25HWE0034).

Institutional Review Board Statement: Not applicable.

Informed Consent Statement: Not applicable.

Data Availability Statement: Data are contained within the article or Supplementary Material.

Acknowledgments: The computational work for this article was partially performed on resources of the National Supercomputing Centre, Singapore (https://www.nscc.sg).

Conflicts of Interest: The funders had no role in the design of the study; in the collection, analyses, or interpretation of data; in the writing of the manuscript; or in the decision to publish the results. Author L.Z. and S.G. were employed by the company P&G. The remaining authors declare that the research was conducted in the absence of any commercial or financial relationships that could be construed as a potential conflict of interest.

References

1. Lau, J.L.; Dunn, M.K. Therapeutic Peptides: Historical Perspectives, Current Development Trends, and Future Directions. *Bioorganic Med. Chem.* **2018**, *26*, 2700–2707. [CrossRef] [PubMed]
2. Apostolopoulos, V.; Bojarska, J.; Chai, T.-T.; Elnagdy, S.; Kaczmarek, K.; Matsoukas, J.; New, R.; Parang, K.; Lopez, O.P.; Parhiz, H.; et al. A Global Review on Short Peptides: Frontiers and Perspectives. *Molecules* **2021**, *26*, 430. [CrossRef] [PubMed]
3. Sharma, K.; Sharma, K.K.; Sharma, A.; Jain, R. Peptide-Based Drug Discovery: Current Status and Recent Advances. *Drug Discov. Today* **2023**, *28*, 103464. [CrossRef] [PubMed]
4. Liu, H.; Duan, Z.; Tang, J.; Lv, Q.; Rong, M.; Lai, R. A Short Peptide from Frog Skin Accelerates Diabetic Wound Healing. *FEBS J.* **2014**, *281*, 4633–4643. [CrossRef] [PubMed]
5. Lee, Y.C.J.; Javdan, B.; Cowan, A.; Smith, K. More than Skin Deep: Cyclic Peptides as Wound Healing and Cytoprotective Compounds. *Front. Cell Dev. Biol.* **2023**, *11*, 1195600. [CrossRef] [PubMed]

6. Chang, H.; Tao, K.; Yang, Y.; Wang, Y.; Ge, M.; Wang, X.; Tang, S.; Yu, H. Novel Cyclized Hexapeptide-9 Outperforms Retinol Against Skin Aging: A Randomized, Double-Blinded, Active- and Vehicle-Controlled Clinical Trial. *J. Cosmet. Dermatol.* **2025**, *24*, e70290. [CrossRef] [PubMed]
7. Pintea, A.; Manea, A.; Pintea, C.; Vlad, R.-A.; Bîrsan, M.; Antonoaea, P.; Rédai, E.M.; Ciurba, A. Peptides: Emerging Candidates for the Prevention and Treatment of Skin Senescence: A Review. *Biomolecules* **2025**, *15*, 88. [CrossRef] [PubMed]
8. Liu, L.; Zhang, L.; Liu, Z.; Tan, C.; Lam, E.; Ehrman, M.C.; Chng, C.-P.; Gupta, S.; Huang, C.; Chen, Y.; et al. Development of a Novel Peptide-Caffeic Acid Conjugate with Enhanced Anti-Photoaging Properties: Efficacy, Transdermal Permeation, and Stability. *Cosmetics* **2026**, *13*, 24. [CrossRef]
9. Zhang, Q.; Hu, C.; Chen, Y.; Chen, Y.; Guo, C.; Liu, Z.; Ding, W. Dual-Targeting Oligopeptide-215 Regulates Skin Barrier Homeostasis Through Concurrent Modulation of JAK—STAT and NF-κB Signaling. *J. Cosmet. Dermatol.* **2026**, *25*, e70704. [CrossRef] [PubMed]
10. Elias, P.M.; Goerke, J.; Friend, D.S. Mammalian Epidermal Barrier Layer Lipids: Composition and Influence on Structure. *J. Investig. Dermatol.* **1977**, *69*, 535–546. [CrossRef] [PubMed]
11. Madison, K.C. Barrier Function of the Skin: "La Raison d'Être" of the Epidermis. *J. Investig. Dermatol.* **2003**, *121*, 231–241. [CrossRef] [PubMed]
12. Elias, P.M. Epidermal Lipids, Barrier Function, and Desquamation. *J. Investig. Dermatol.* **1983**, *80*, S44–S49. [CrossRef] [PubMed]
13. Wang, E.; Klauda, J.B. Structure and Permeability of Ceramide Bilayers and Multilayers. *J. Phys. Chem. B* **2019**, *123*, 2525–2535. [CrossRef] [PubMed]
14. Masukawa, Y.; Narita, H.; Shimizu, E.; Kondo, N.; Sugai, Y.; Oba, T.; Homma, R.; Ishikawa, J.; Takagi, Y.; Kitahara, T.; et al. Characterization of Overall Ceramide Species in Human Stratum Corneum. *J. Lipid Res.* **2008**, *49*, 1466–1476. [CrossRef] [PubMed]
15. Van Smeden, J.; Boiten, W.A.; Hankemeier, T.; Rissmann, R.; Bouwstra, J.A.; Vreeken, R.J. Combined LC/MS-Platform for Analysis of All Major Stratum Corneum Lipids, and the Profiling of Skin Substitutes. *Biochim. Biophys. Acta Mol. Cell Biol. Lipids* **2014**, *1841*, 70–79. [CrossRef] [PubMed]
16. Law, S.; Wertz, P.W.; Swartzendruber, D.C.; Squier, C.A. Regional Variation in Content, Composition and Organization of Porcine Epithelial Barrier Lipids Revealed by Thin-Layer Chromatography and Transmission Electron Microscopy. *Arch. Oral Biol.* **1995**, *40*, 1085–1091. [CrossRef] [PubMed]
17. Weerheim, A.; Ponec, M. Determination of Stratum Corneum Lipid Profile by Tape Stripping in Combination with High-Performance Thin-Layer Chromatography. *Arch. Dermatol. Res.* **2001**, *293*, 191–199. [CrossRef] [PubMed]
18. Bos, J.D.; Meinardi, M.M.H.M. The 500 Dalton Rule for the Skin Penetration of Chemical Compounds and Drugs. *Exp. Dermatol.* **2000**, *9*, 165–169. [CrossRef] [PubMed]
19. Silva, T.; Oliveira, C.; Borges, F. Caffeic Acid Derivatives, Analogs and Applications: A Patent Review (2009–2013). *Expert Opin. Ther. Pat.* **2014**, *24*, 1257–1270. [CrossRef] [PubMed]
20. Jesus, A.; Ratanji, S.; Cidade, H.; Sousa, E.; Cruz, M.T.; Oliveira, R.; Almeida, I.F. Phenolics as Active Ingredients in Skincare Products: A Myth or Reality? *Molecules* **2025**, *30*, 1423. [CrossRef] [PubMed]
21. Monje-Galvan, V.; Klauda, J.B. Preferred Binding Mechanism of Osh4's Amphipathic Lipid-Packing Sensor Motif, Insights from Molecular Dynamics. *J. Phys. Chem. B* **2018**, *122*, 9713–9723. [CrossRef] [PubMed]
22. Talandashti, R.; Mahdiuni, H.; Jafari, M.; Mehrnejad, F. Molecular Basis for Membrane Selectivity of Antimicrobial Peptide Pleurocidin in the Presence of Different Eukaryotic and Prokaryotic Model Membranes. *J. Chem. Inf. Model.* **2019**, *59*, 3262–3276. [CrossRef] [PubMed]
23. Chng, C.-P.; Cho, N.-J.; Hsia, K.J.; Huang, C. Role of Membrane Stretch in Adsorption of Antiviral Peptides onto Lipid Membranes and Membrane Pore Formation. *Langmuir* **2021**, *37*, 13390–13398. [CrossRef] [PubMed]
24. Shamaprasad, P.; Frame, C.O.; Moore, T.C.; Yang, A.; Iacovella, C.R.; Bouwstra, J.A.; Bunge, A.L.; McCabe, C. Using Molecular Simulation to Understand the Skin Barrier. *Prog. Lipid Res.* **2022**, *88*, 101184. [CrossRef] [PubMed]
25. Shamaprasad, P.; Moore, T.C.; Xia, D.; Iacovella, C.R.; Bunge, A.L.; McCabe, C. Multiscale Simulation of Ternary Stratum Corneum Lipid Mixtures: Effects of Cholesterol Composition. *Langmuir* **2022**, *38*, 7496–7511. [CrossRef] [PubMed]
26. Gupta, R.; Sridhar, D.B.; Rai, B. Molecular Dynamics Simulation Study of Permeation of Molecules through Skin Lipid Bilayer. *J. Phys. Chem. B* **2016**, *120*, 8987–8996. [CrossRef] [PubMed]
27. Lee, C.T.; Comer, J.; Herndon, C.; Leung, N.; Pavlova, A.; Swift, R.V.; Tung, C.; Rowley, C.N.; Amaro, R.E.; Chipot, C.; et al. Simulation-Based Approaches for Determining Membrane Permeability of Small Compounds. *J. Chem. Inf. Model.* **2016**, *56*, 721–733. [CrossRef] [PubMed]
28. Lundborg, M.; Wennberg, C.L.; Narangifard, A.; Lindahl, E.; Norlén, L. Predicting Drug Permeability through Skin Using Molecular Dynamics Simulation. *J. Control. Release* **2018**, *283*, 269–279. [CrossRef] [PubMed]
29. Chng, C.P.; Zhang, L.; Gupta, S.; Huang, C. Palmitoylation Enhances Short Polar Peptide Permeation across Stratum Corneum Lipid Bilayer: A Molecular Dynamics Study. *Extrem. Mech. Lett.* **2024**, *71*, 102213. [CrossRef]

30. Martinez, L.; Andrade, R.; Birgin, E.G.; Martinez, J. Packmol: A Package for Building Initial Configurations for Molecular Dynamics Simulations. *J. Comput. Chem.* **2009**, *30*, 2157–2164. [CrossRef] [PubMed]
31. Jo, S.; Kim, T.; Iyer, V.G.; Im, W. CHARMM-GUI: A Web-Based Graphical User Interface for CHARMM. *J. Comput. Chem.* **2008**, *29*, 1859–1865. [CrossRef] [PubMed]
32. Lee, J.; Cheng, X.; Swails, J.M.; Yeom, M.S.; Eastman, P.K.; Lemkul, J.A.; Wei, S.; Buckner, J.; Jeong, J.C.; Qi, Y.; et al. CHARMM-GUI Input Generator for NAMD, GROMACS, AMBER, OpenMM, and CHARMM/OpenMM Simulations Using the CHARMM36 Additive Force Field. *J. Chem. Theory Comput.* **2016**, *12*, 405–413. [CrossRef] [PubMed]
33. Abraham, M.J.; Murtola, T.; Schulz, R.; Páll, S.; Smith, J.C.; Hess, B.; Lindahl, E. GROMACS: High Performance Molecular Simulations through Multi-Level Parallelism from Laptops to Supercomputers. *SoftwareX* **2015**, *1*, 19–25. [CrossRef]
34. Páll, S.; Abraham, M.J.; Kutzner, C.; Hess, B.; Lindahl, E. Tackling Exascale Software Challenges in Molecular Dynamics Simulations with GROMACS. In *Proceedings of the Solving Software Challenges for Exascale*; Markidis, S., Laure, E., Eds.; Springer: Cham, Switzerland, 2015; pp. 3–27.
35. Pronk, S.; Páll, S.; Schulz, R.; Larsson, P.; Bjelkmar, P.; Apostolov, R.; Shirts, M.R.; Smith, J.C.; Kasson, P.M.; van der Spoel, D.; et al. GROMACS 4.5: A High-Throughput and Highly Parallel Open Source Molecular Simulation Toolkit. *Bioinformatics* **2013**, *29*, 845–854. [CrossRef] [PubMed]
36. Badhe, Y.; Gupta, R.; Rai, B. Structural and Barrier Properties of the Skin Ceramide Lipid Bilayer: A Molecular Dynamics Simulation Study. *J. Mol. Model.* **2019**, *25*, 140. [CrossRef] [PubMed]
37. Venable, R.M.; Brown, F.L.H.; Pastor, R.W. Mechanical Properties of Lipid Bilayers from Molecular Dynamics Simulation. *Chem. Phys. Lipids* **2015**, *192*, 60–74. [CrossRef] [PubMed]
38. Feller, S.E.; Pastor, R.W. Constant Surface Tension Simulations of Lipid Bilayers: The Sensitivity of Surface Areas and Compressibilities. *J. Chem. Phys.* **1999**, *111*, 1281–1287. [CrossRef]
39. Bernhardt, N.; Faraldo-Gómez, J.D. MOSAICS: A Software Suite for Analysis of Membrane Structure and Dynamics in Simulated Trajectories. *Biophys. J.* **2023**, *122*, 2023–2040. [CrossRef] [PubMed]
40. Somboon, K.; Chng, C.P.; Huang, C.; Gupta, S. Enhancing Niacinamide Skin Penetration via Other Skin Brightening Agents: A Molecular Dynamics Simulation Study. *Int. J. Mol. Sci.* **2025**, *26*, 1555. [CrossRef] [PubMed]
41. Mortazavi, S.M.; Moghimi, H.R. Skin Permeability, a Dismissed Necessity for Anti-wrinkle Peptide Performance. *Int. J. Cosmet. Sci.* **2022**, *44*, 232–248. [CrossRef] [PubMed]
42. Veiga, E.; Ferreira, L.; Correia, M.; Pires, P.C.; Hameed, H.; Araújo, A.R.T.S.; Cefali, L.C.; Mazzola, P.G.; Hamishehkar, H.; Veiga, F.; et al. Anti-Aging Peptides for Advanced Skincare: Focus on Nanodelivery Systems. *J. Drug Deliv. Sci. Technol.* **2023**, *89*, 105087. [CrossRef]
43. Villanueva, M.E.; Troncoso, J.; Losada-Pérez, P.; Jover, A. Impact of Amylenes in Dipeptide-Mediated Phospholipid Vesicle Integrity and Aggregation. *J. Mol. Liq.* **2025**, *437*, 128596. [CrossRef]
44. Duan, Q.; Ye, Z.; Zhou, K.; Wang, F.; Lian, C.; Shang, Y.; Liu, H. An Investigation into the Transdermal Behavior of Active Ingredients by Combination of Experiments and Multiscale Simulations. *J. Phys. Chem. B* **2024**, *128*, 6327–6337. [CrossRef] [PubMed]
45. Mao, G.; VanWyck, D.; Xiao, X.; Mack Correa, M.C.; Gunn, E.; Flach, C.R.; Mendelsohn, R.; Walters, R.M. Oleic Acid Disorders Stratum Corneum Lipids in Langmuir Monolayers. *Langmuir* **2013**, *29*, 4857–4865. [CrossRef] [PubMed]

Disclaimer/Publisher's Note: The statements, opinions and data contained in all publications are solely those of the individual author(s) and contributor(s) and not of MDPI and/or the editor(s). MDPI and/or the editor(s) disclaim responsibility for any injury to people or property resulting from any ideas, methods, instructions or products referred to in the content.